Sensors & Actuators: B. Chemical 324 (2020) 128667

Contents lists available at ScienceDirect

Sensors and Actuators: B. Chemical

journal homepage: www.elsevier.com/locate/snb

Characterization of a modular microfluidic photoionization detector

Gustavo Coelho Rezende [a], Stéphane Le Calvé [b,c], Jürgen J. Brandner [d], David Newport [a,*]

[a] Bernal Institute, School of Engineering, University of Limerick, V94 T9PX, Limerick, Ireland
[b] Institut de Chimie et Procédé pour l'Energie, l'Environnement et la Santé (ICPEES, UMR 7515 CNRS/Unistra), Group of Atmospheric Physical Chemistry, 25 rue Becquerel, 67087, Strasbourg, Cedex 02, France
[c] In'Air Solutions, 25 rue Becquerel, 67000, Strasbourg, France
[d] Institute of Microstructure Technology (IMT), Karlsruhe Institute of Technology, Germany

ARTICLE INFO

Keywords:
Photoionization detector
Miniaturization
Microfabrication
Gas chromatography
VOC detection
Air quality

ABSTRACT

Photoionization detectors with a small ionization chamber can contribute to overall gas analyser miniaturization. This work reports the characterization of a microfluidic photoionization detector prototype (μPID) which is constructed to be modular for easy replacement of the components and maintenance. The device is fabricated by micromilling and electrical discharge machining, dispensing clean room fabrication techniques. The μPID ionization chamber is a microchannel and four channel designs are presented and tested in experiments in order to evaluate the influence of the geometrical parameters on the detector performance. The chamber volumes of the channel designs range from 1.1 to 6.7 μL. Experimental characterization of the prototype is performed when it is used without and with a portable gas chromatograph (GC) for volatile organic compounds (VOCs) analysis. When a sample of 100 ppm toluene is injected directly into the μPID, it can generate a current signal up to ~4 nA. When used without a GC, the device showed a linear response for an injection of toluene gas concentrations ranging from 1 to 100 ppm. A combination of high illumination area and electrode area resulted in the highest signal in the μPID with a detection limit of ~40 ppb of toluene. When integrated to the portable GC, the detection limit reached for toluene is ~140 ppb. The detection limit for toluene was further reduced to low ppb levels (~5 ppb) when a preconcentrator was integrated into the sampling loop of the portable GC.

1. Introduction

Indoor environments, where people spend close to 90 % of their time [1,2], can have Volatile Organic Compounds (VOCs) contaminating the air. VOCs are a class of carbon-containing chemicals with a high vapour pressure at ambient temperature. Those chemicals are released by varnishes, paints, solvents, cleaning materials, etc. In addition, outdoor VOCs emission from automobile or industrial waste can contribute to indoor pollution [3]. Many VOCs can cause health problems, including benzene, which is carcinogenic and has no safe recommended level of exposure [4,5]. Those facts raised the awareness of authorities in many countries, which issued regulations to limit the exposure to such chemicals [6,7].

Photoionization detectors (PIDs) can measure the presence of VOCs in air samples. They measure the photoionization current generated when the VOCs are hit by photons with larger energy than the molecule ionization potential [8]. The PID is a concentration sensitive detector, the current generated being proportional to the concentration of VOCs inside its ionization chamber [8]. The main components of the detector are: 1) ionization source, which emits the high energy light to ionize the sample; 2) electrodes, which generate an electric field for the collection of the electrons and ions; 3) ionization chamber, which is where the gas sample flows through and is detected.

In order to identify the different VOCs present in air samples, the PID can be integrated to a gas chromatograph (GC). This type of gas analyser (GC-PID) can separate, identify and quantify different chemicals. Commercial GC-PIDs with low detection limit are still lab-based, slow, bulky and heavy [9–11]; therefore, not ideal to comply with the recent regulations demands which require portability and fast analysis. An efficient gas analyser with low resource consumption, improved robustness, high analysis speed, low cost, improved portability and low detection limit can be produced with miniaturization of the main GC components, including the detector.

An important part of the PID to be miniaturized is the ionization chamber, whose volume influences directly the response time. In addition, a small ionization chamber allows a reduction in the sample

* Corresponding author.
E-mail address: david.newport@ul.ie (D. Newport).

https://doi.org/10.1016/j.snb.2020.128667
Received 10 March 2020; Received in revised form 5 July 2020; Accepted 28 July 2020
Available online 7 August 2020

volume without depleting the signal intensity. With a smaller sample volume, at a constant sample flow rate, it is possible to have a faster analysis time and increase the autonomy of the carrier gas cylinder used with the GC-PID; thus, increasing the portability of the gas analyser. Commercial PIDs are not ideal for a miniaturized gas analyser since they have a large ionization chamber, with volumes ranging from 50 to 100 µL [12–16]. Some commercial PIDs can have small external size (20 mm) but they have an ionization chamber whose design is not optimized for integration into a portable gas analyser due to the presence of a membrane which can delay the fill time of the ionization chamber [14,17].

Recent developments in PID miniaturization produced devices with ionization chamber volume close to 1 µL [18–23]. The new designs used mostly lithography based fabrication techniques with silicon and glass as main materials. As an alternative to those fabrication techniques, Rezende et al. [24] proposed a µPID fabricated by micromilling and electrical discharge machining. The main features of this design were its relatively low prototyping cost, no need for clean room or photomasks for fabrication, and its modular construction, allowing easy replacement of the components and maintenance of the detector. The present work shows the characterization of the µPID previously described by Rezende et al. [24], including experiments without and with a portable GC. Four ionization chamber geometries shaped as microchannels are evaluated; the performance of the GC-µPID is investigated and compared to a commercial PID integrated to the same portable GC system. In addition, the µPID response is evaluated when a preconcentrator (PC) is integrated into the GC sampling loop.

2. Experimental setup and materials

2.1. Chemicals

Main chemicals used in the experiments are: 1) Nitrogen gas at 99.99 % purity; 2) Toluene gas mixture in nitrogen at 10 ppm and 100 ppm; 3) BTEX mixture with nitrogen as balance gas containing either 5 ppb or 10 ppm of benzene, toluene, ethylbenzene, o-xylene, m-xylene, p-xylene.

2.2. Microchannels designs

The µPID design tested for this work is detailed in Rezende et al. [24]. The ionization chamber of the µPID is a microchannel and Fig. 1 shows the design of the four microchannel geometries used inside the detector (channel A, B, C and D). The channel designs presented have the objective to investigate the influence of channel geometry on the detector performance. Fig. 2 presents the geometrical parameters of the microchannel, which are: channel width (W), height (H), length (L), illumination area (A_i), electrode area (A_e) and ionization chamber

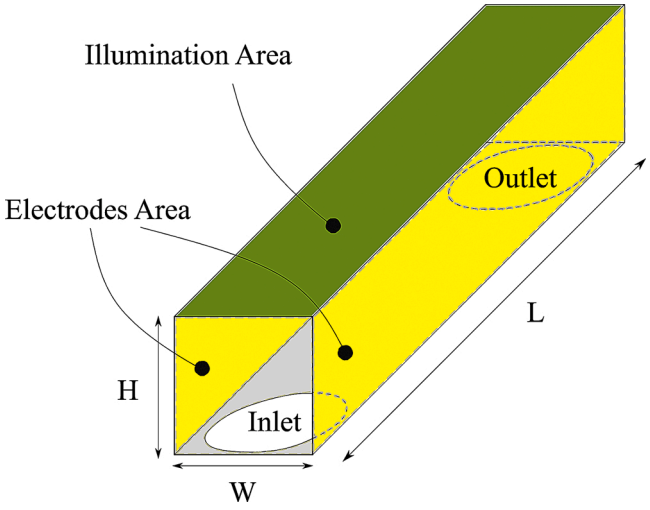

Fig. 2. Main microchannel geometrical parameters.

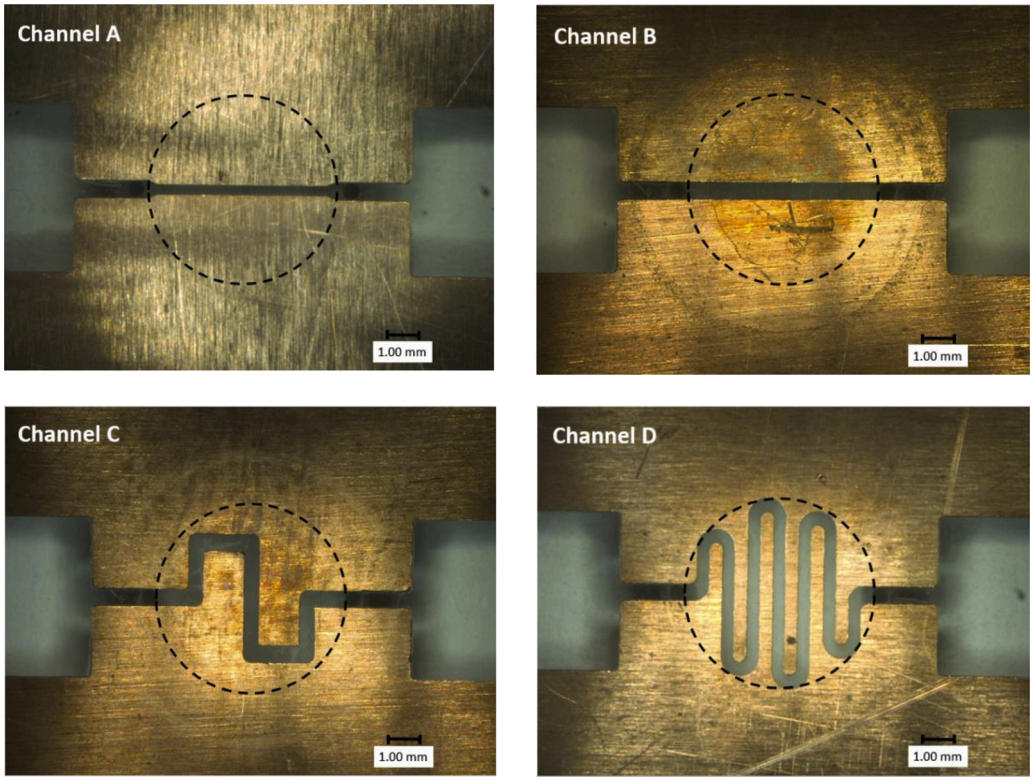

Fig. 1. Microchannel designs used in the µPID (channel A, B, C and D).

volume (V_c).

In theory, the geometrical parameters influence the μPID performance as following: 1) Width (W): equals the distance between the copper electrodes; therefore, it is inversely proportional to the electric field intensity, and consequently, to the detector sensitivity; 2) Height (H): shallow channels yield more uniform sample ionization, but less electrode area; 3) Length (L): for the microchannel design, the length influences the electrode area, illumination area and ionization chamber volume; 4) Electrode area (A_e): depends on the shape and the height of the microchannel and it is directly proportional to sensitivity; 5) Lamp illumination area (A_i): top surface of the channel illuminated by the UV lamp. Higher illumination area means more ionized molecules; and 6) Ionization chamber volume (V_c): volume of the microchannel from inlet to outlet. Large volumes can deplete the signal if the sample volume is small compared to the chamber volume (Supplementary material S.4).

From channel A to B, the main objective is to evaluate the effect of width change, which modifies the illumination area and ionization chamber volume consequently, but keeps a constant electrode area. Channels B, C and D are designed to investigate the influence of increased illumination area and electrode area. Notice that the width of channel D is 400 μm instead of 500 μm (as in channel B and C), this was done so that the channel D ionization chamber would fit inside the lamp illumination diameter, which is 6 mm as indicated by the dashed circle on all microchannels in Fig. 1. Table 1 gives the values of the geometries for all the channels. Notice that channel D has electrode area of 32.6 mm^2 at least 4 times higher than channels A and B. In addition, the illumination area of 13.3 mm^2 of channel D is around 6 and 4 times higher than those values for channels A and B, respectively. With a value of 6.7 μL, channel D has the highest ionization chamber volume, almost 7 times higher than the chamber volume of channel A.

2.3. Setup for direct injection into μPID

Fig. 3 shows an experimental setup built to evaluate the μPID prototype. Two gas sample supplies are used, one containing a VOC pollutant and another with nitrogen. Both are isolated by ball valves (BV1 and BV2) and connected to a mass flow controller (MFC). The MFC regulates the flow rate of gas sample into the μPID and the flow rate leaving the device is read by a mass flow meter (MFM). The MFC and MFM (F-100D-AAD-33-V) are from Bronkhorst and the model of MFC used varies depending on the flow rate required for the experiment. All tubing connecting the gas flow are made of PTFE. For safety reasons, the experimental setup is installed inside a fume hood to avoid spreading of the pollutant gases into the test room. At the exit of the fluidic path, the gas sample is left to atmospheric pressure.

The μPID 10.6 eV lamp is powered by the UV lamp drive circuit from a commercial PID (piD-TECH® eVx™, 045-010), which is supplied with 4 V and 35 mA from the power supply 1. To measure the current inside the ionization chamber, the power supply 2 applies a voltage between the copper electrodes (30 V), and the current generated by the PID detection goes through the current preamplifier (Low-Noise Current Preamplifier, Stanford Research Systems, SR570), which can filter and amplify low current signals. After amplifying the current signal to voltage signal, the voltage magnitude is measured by an analog-to-digital converter (ADC) from National Instruments (NI-USB-6001). A MATLAB algorithm reads and stores the digital signal in a computer. Due to the low magnitude of the current measured, a Faraday cage enclosing the μPID is used in the experiments to mitigate electromagnetic noise influence.

Table 1
Magnitude of the microchannels geometrical parameters.

Parameter		Channel A	Channel B	Channel C	Channel D
H	[mm]	0.50	0.50	0.50	0.50
W	[mm]	0.25	0.50	0.50	0.40
L	[mm]	7.0	7.0	14.0	32.9
A_e	[mm^2]	7.0	7.0	12.9	32.6
A_i	[mm^2]	2.2	3.5	6.9	13.3
V_c	[μL]	1.1	1.8	3.5	6.7

2.4. Setup of μPID coupled to GC for BTEX separation

The μPID is also tested with a portable GC [25] by substituting the commercial PID (Baseline MOCON, piD-TECH Blue, part number 045-014) for the μPID; yielding a GC-μPID system with the schematic shown in Fig. 4a. The analyser works in three steps: sampling, separation and detection. A BTEX gas mixture is connected to the inlet of the gas analyser which uses a mini diaphragm air pump (270 EC, Schwarzer) and a solenoid 6-ports valve (MTV-6LL-N32UF-1, Takasago) equipped with a PEEK 200 μL sampling loop which is filled with the sample and then injected into the column for analysis as described in Fig. 4b and c.

At the sampling stage illustrated by Fig. 4b, the gas sample is directed to a waste, so that the 200 μL sampling loop is filled with the gaseous pollutant mixture, which occurs in less than 10 s. After filling the sampling loop with a BTEX mixture, the injection stage can start. The injection is initiated by the BTEX analyser controller panel, and makes the valve switch position to reach the configuration displayed in Fig. 4c, so that the carrier gas pushes the sample downstream. The optimal time for the injection stage was verified in previous studies and is 20 s [25].

The 6-ports valve is connected directly to the separation column to minimize dead volume. The separation column is a 20 m long capillary from Restek with RXi-624 stationary phase and 1 μm film thickness. Internal and external diameters are 0.18 mm and 0.74 mm, respectively. The separation column is coiled in a 7.5 cm diameter inside a 10 cm × 10 cm × 1 cm aluminium plate which serves as an oven. It is heated by an electric resistor that controls the temperature with a commercial controller (CAL 3300). To improve the oven performance the column is covered by a 2 cm thick cork insulation layer. The temperature set at the column for all the experiments is 65 °C and is constant for the analysis duration (isocratic mode).

The μPID is located in the outlet of the separation column (Fig. 4a). The electronic connections for the μPID operation are the same as demonstrated in Fig. 3, and a MFM can be placed after the separation column and the μPID to verify the absence of leakage. The flow rate through the system is ensured by the pressure regulator (PR) from Bronkhorst, set at 4 bars, which yield a flow rate measured at the end of the separation column of 2.39 mL_n/min.

3. Results for sample direct injection into the μPID

3.1. Influence of microchannel design

In order to verify the influence of different microchannel designs on the detector signal, the response using channels A, B, C and D were obtained with direct injection of nitrogen and 100 ppm of toluene (nitrogen balance gas) at 50 mL_n/min. Fig. S1 shows the signal (current measurement) as a function of time for all channels. For each channel, three datasets (n = 3) measured in a sequence are shown to demonstrate the repeatability of the results (black, red and blue lines). The signal was obtained by applying 30 V on the signal electrodes. The current preamplifier was set for a low-pass first order RC filter with cut-off frequency (f_c) of 10 Hz, 12 dB attenuation and 1 nA/V amplification. The amplification and attenuation values used in the preamplifier will remain constant for all results obtained in this work.

The following procedure was used to obtain the signal: i) channel purged with nitrogen during 5 min; ii) Start the data acquisition (t = 0 s on the plots of Fig. S1) and continue the purge with nitrogen for 1 min; iii) Close nitrogen supply valve and wait for the MFC to measure 0 mL_n/min (which lasts about 1 min); iv) at 2 min of test, open the toluene 100 ppm connection valve for pollutant signal acquisition during 3 min;

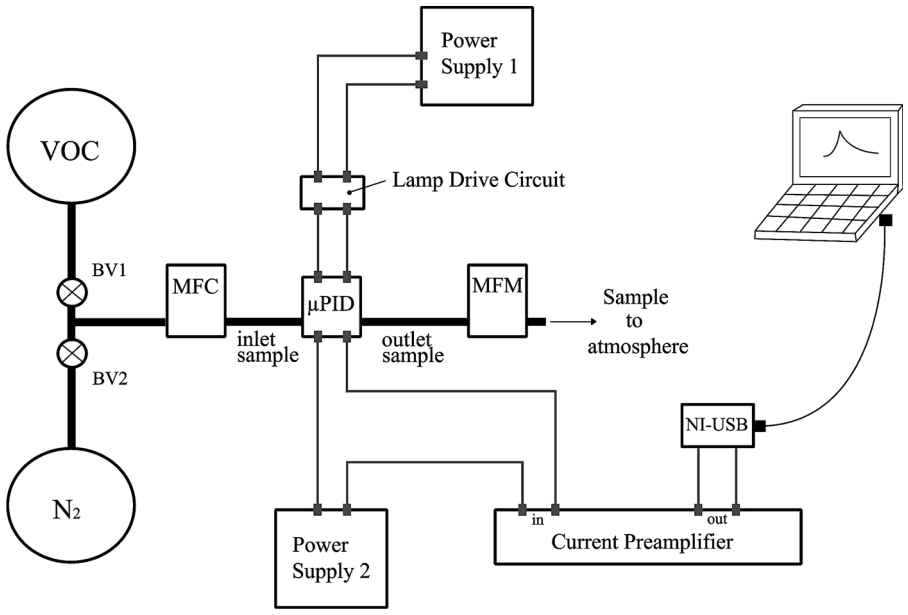

Fig. 3. Experimental setup used for the experiments with the μPID.

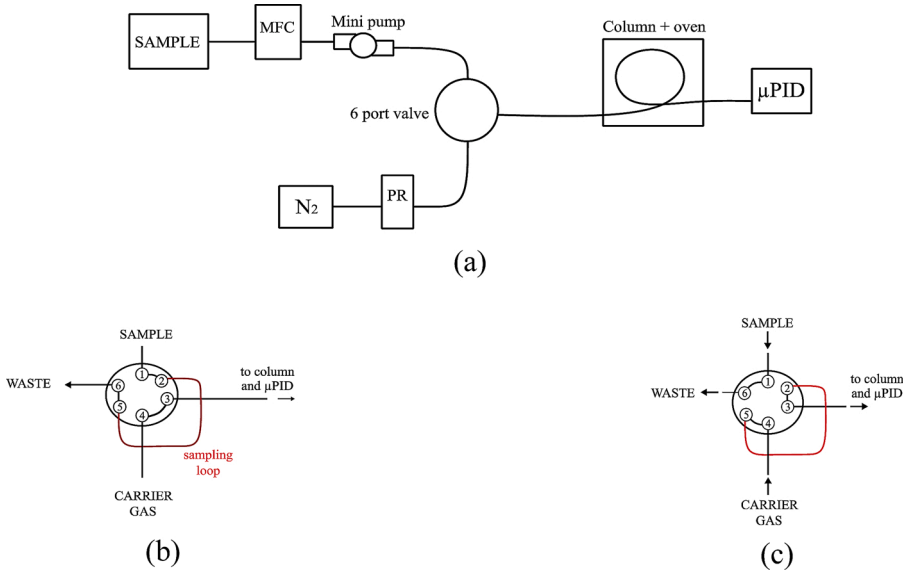

Fig. 4. Schematics of the experiment integrating the μPID with a portable GC. a) Setup main components, including pressure regulator (PR) and mass flow controller (MFC); b) 6-ports valve sampling stage; c) 6-ports valve analysis stage.

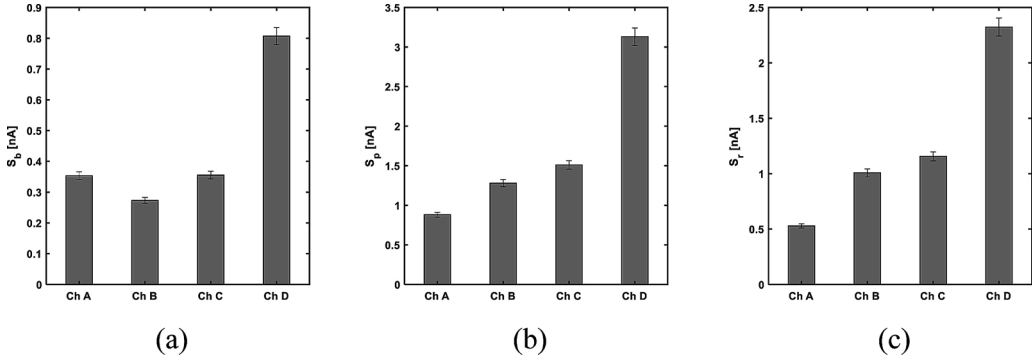

Fig. 5. Average signal level for all channels. a) Baseline signal (S_b); b) Pollutant signal (S_p); c) Signal rise (S_r).

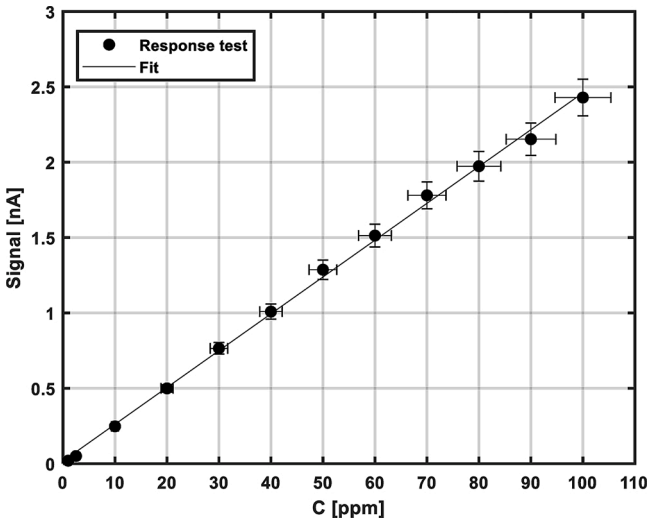

Fig. 6. Channel D response curve for 1 to 100 ppm toluene concentration range at 30 V and 20 mLn/min. Vertical error bar is 3.5 %, which stems from the maximum error observed in the experiments for direct injection of sample. The horizontal error bar varies from 5 % to 12.5 %, where the highest error is obtained for lowest concentration. This value range is obtained by the toluene gas cylinder concentration error and from the mixing of nitrogen and toluene flows that yielded the dilution.

v) close the toluene 100 ppm valve and wait for the MFC to display 0 mL_n/min; vi) open the nitrogen valve to purge the channel so that the signal level returns to the baseline.

For each dataset, the signal representing the stable value for the baseline (S_b) and the pollutant (S_p) are obtained at 35 s and 270 s of experiment, respectively. The signal at 35 and 270 s is considered stable with less than 0.2 % variation in a 5 s interval. The difference between the pollutant and the baseline signal is the signal rise:

$$S_r = S_p - S_b. \quad (1)$$

The average value of the signal at the baseline (S_b), pollutant (S_p) and rise (S_r) level for all channels are displayed in Fig. 5. The S_r is what ultimately permits to estimate the sensitivity level of the detector. As illustrated by Fig. 5b and c, the highest variation for S_p and S_r is found between channel A and D, where the channel D can have values up to 3 times higher. Regarding S_b (see Fig. 5a), the largest difference is found between channel B and D, where the baseline of channel D is higher than double the channel B baseline. The error bars displayed in Fig. 5 are 3.5 % of the measured value. This error value stems from the maximum error observed in the experiments for direct injection of sample. The response time, which is the time it takes for the signal to go from baseline level to pollutant level, is less than 1 s for all channels.

Table 1 can be used as a reference to investigate the influence on the measured signal caused by the geometry changes of each channel. From channel A to channel B, the signal level doubles and the main geometrical change between those two designs is the width of the channel (W), which changes the illumination area (A_i) consequently. The change in the two parameters, W and A_i, observed from channel A to channel B have opposite effects on the signal level. Channel A has smaller W which means it has a stronger electric field compared to channel B, this increases the ion and electron collection efficiency and contributes positively for the sensitivity of the detector. On the other hand, channel B, despite the larger W, has a larger illumination area (A_i), which also contributes positively to the sensitivity of the μPID. The increase in signal rise (S_r) from channel A to B observed in Fig. 5c shows that, for the investigated channel dimensions, illumination area is more important than width for signal level.

Fig. 5a shows that the baseline level for channel A is higher than channel B, which is likely caused by a larger portion of the electrodes being hit by photons on channel A. For channels A, B, C and D, the portion of the electrodes top surface illuminated by the lamp diminishes with increasing ionization chamber volume; however, for channels B, C and D, baseline signal increases with less electrode surface area illuminated by the lamp and channel A has an inverse effect. An explanation for this phenomenon can be that channels B, C and D generate higher current for the residual ionisable chemical components that can be inside the ionization chamber even when nitrogen is used, since those channel designs have higher sensitivity due to the larger electrode area and illumination area compared to channel A.

For channels B, C and D, it is possible to attribute the increase in signal rise (S_r) to the simultaneous increase in illumination area and electrode area. A change in channel D compared to channels B and C is the width, which is 100 μm lower compared to channels B and C. This has also a positive impact in the channel D sensitivity and has contributed to establish it as the most sensitive channel design from the four presented in this work. Because of the changes in the channel shapes, ionization chamber volume increases as illumination area increases. V_c variation should not have a significant impact on the signal presented in Fig. 5 because the PID is a concentration sensitive detector. A V_c variation can cause signal intensity change if the sample volume is small compared to the ionization chamber volume (see Supplementary material S.4).

3.2. Calibration curve and detection limit

A range of toluene concentrations (1–100 ppm) were injected into the μPID to obtain a response curve. The detector (using channel D) was subjected to a series of gas purge with nitrogen followed by injection of toluene. The range of concentrations were achieved by diluting the concentration level of the toluene 100 ppm gas cylinder with a mixed nitrogen flow. The nitrogen and toluene flow rates summed up 20 mL_n/min and a potential of 30 V was applied on the electrodes to yield fast stabilization and a stable signal, respectively.

The μPID signal rise (S_r) as a function of toluene concentration (C) at the range 1–100 ppm follows a linear growth, as indicated in Fig. 6, which is estimated from a linear fit function with forced zero intercept. The linear fit function angular coefficient (a) and the coefficient of determination (r^2) are 24.67 pA/ppm and 0.9997, respectively. The concentration uncertainty presented in Fig. 6 is obtained from the toluene gas cylinder concentration error and from the mixing of nitrogen and toluene flows that yielded the dilution. The resulting concentration uncertainty has values from 5 to 12.5 % at the highest and lowest concentrations, respectively.

The detection limit in concentration units of the μPID (C_{DL}) is defined as the concentration that yields a signal rise three times higher than the noise measurement at the baseline (N). Considering the linear nature of the signal for the concentration range measured, C_{DL} can be estimated from the linear fit of the response curve with forced zero intercept, therefore:

$$C_{DL} = (3.N)/a \quad (2)$$

The sensitivity (a), which is also the slope of the linear fit, depends essentially on the design of the device, while the noise can be treated with filters and signal post-processing. The lowest baseline noise measured is 0.3 pA and this noise value was obtained using a low pass first order RC filter from the current preamplifier with a cut-off frequency (f_c) of 0.03 Hz in combination with a digital moving average filter. Considering the lowest baseline noise, the detection limit of toluene is ~40 ppb for the sample direct injection test presented in Fig. 5.

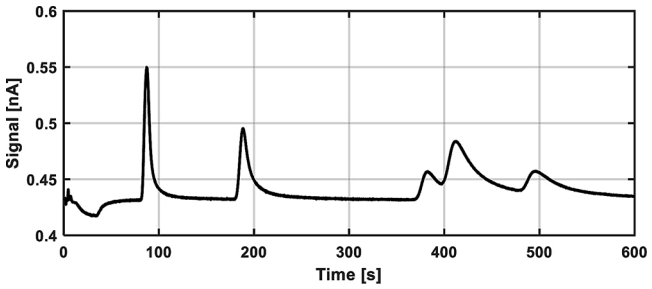

Fig. 7. Chromatogram for 10 ppm BTEX injection using channel D.

4. Results for μPID integrated in the GC

4.1. Influence of microchannel design on the chromatogram and comparison with a commercial PID

Experiments with GC-μPID were also performed for channels A, B, C, D and a commercial portable PID (Baseline MOCON, piD-TECH eVx Green, part number 045-010). The commercial PID tested is not the same one originally used with the portable GC because the original commercial PID had a measurement range (0.5 ppb to 2 ppm) lower than the sample concentrations applied to test the μPID (1 ppm–10 ppm); therefore, it would not be able to read the sample at the same concentration levels injected into the μPID.

Fig. 7 shows the chromatogram with 10 ppm BTEX sample for channel D. The chromatograms for all other channels and the commercial PID are presented in Section S.3 of the Supplementary material. Optimal filter cut-off frequency applied in the μPID, which generated the best signal-to-noise ratio was 0.3 Hz. Retention time for μPID and commercial PID are essentially the same with a difference lower than 1 %. The peaks, in the order that they leave the separation column are: 1st) benzene; 2nd) toluene; 3rd) ethylbenzene; 4th) m-xylene and p-xylene (coelluted in the same peak); 5th) o-xylene. Retention times for benzene, toluene, ethylbenzene, m,p-xylenes and o-xylene peaks are 88 s, 189 s, 382 s, 412 s and 495 s, respectively.

The detection limits of BTEX for all channels and commercial PID are displayed in Fig. 8. Since only the 10 ppm BTEX signal level was measured, the detection limit is estimated assuming a linear response curve with zero intercept. For the microchannels, the noise considered for the detection limit calculation is the same (0.3 pA, the lowest noise) and the detection limit magnitude follows the order $(C_{DL})_{ChA} > (C_{DL})_{ChB} > (C_{DL})_{ChC} > (C_{DL})_{ChD}$. The detection limit for channel D calculated by this way reach values of 72, 127, 429, 316 and 448 ppb of benzene, toluene, ethylbenzene, m,p-xylenes and o-xylene, respectively. Notice that the detection limit of benzene for the μPID channels B (134 ppb), C (107 ppb) and D (72 ppb) are better compared to the commercial PID (157 ppb) whereas the commercial PID exhibits better sensitivity for ethylbenzene and xylenes.

The peak width at half height ($w_{1/2}$) is compared on Fig. 9 for the microchannels and the commercial PID. For the benzene peak, the commercial PID has a negative impact on the width, yielding a slightly larger benzene peak (15 % larger than the channel D, for example). However, for toluene and ethylbenzene, the peak width has no conclusive difference from the microchannels and the commercial PID, because the average differences uncertainties are all overlapped. The xylenes (m, p,o-xylenes) are sharper for the commercial PID. No significant $w_{1/2}$ variation was observed between the microchannel designs, this can be explained by the fact that the volume of the ionization chamber is small compared to the sample volume eluting from the separation column, as analysed in the Supplementary material Section S.4.

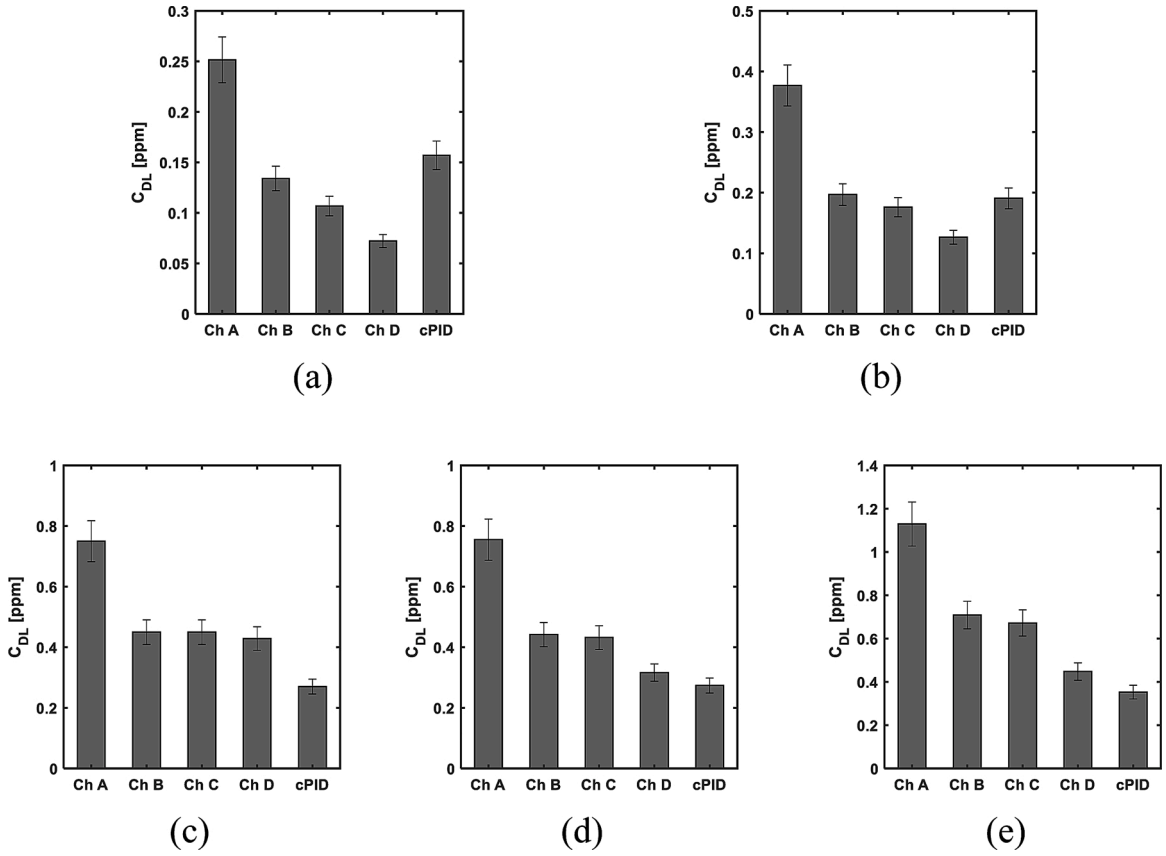

Fig. 8. Estimated concentration detection limit (*CDL*) for all microchannels (30 V) and commercial PID with a 10 ppm BTEX sample: a) benzene, b) toluene, c) ethylbenzene, d) m, p-xylenes and e) o-xylene. Detection limit error is 8.9 %.

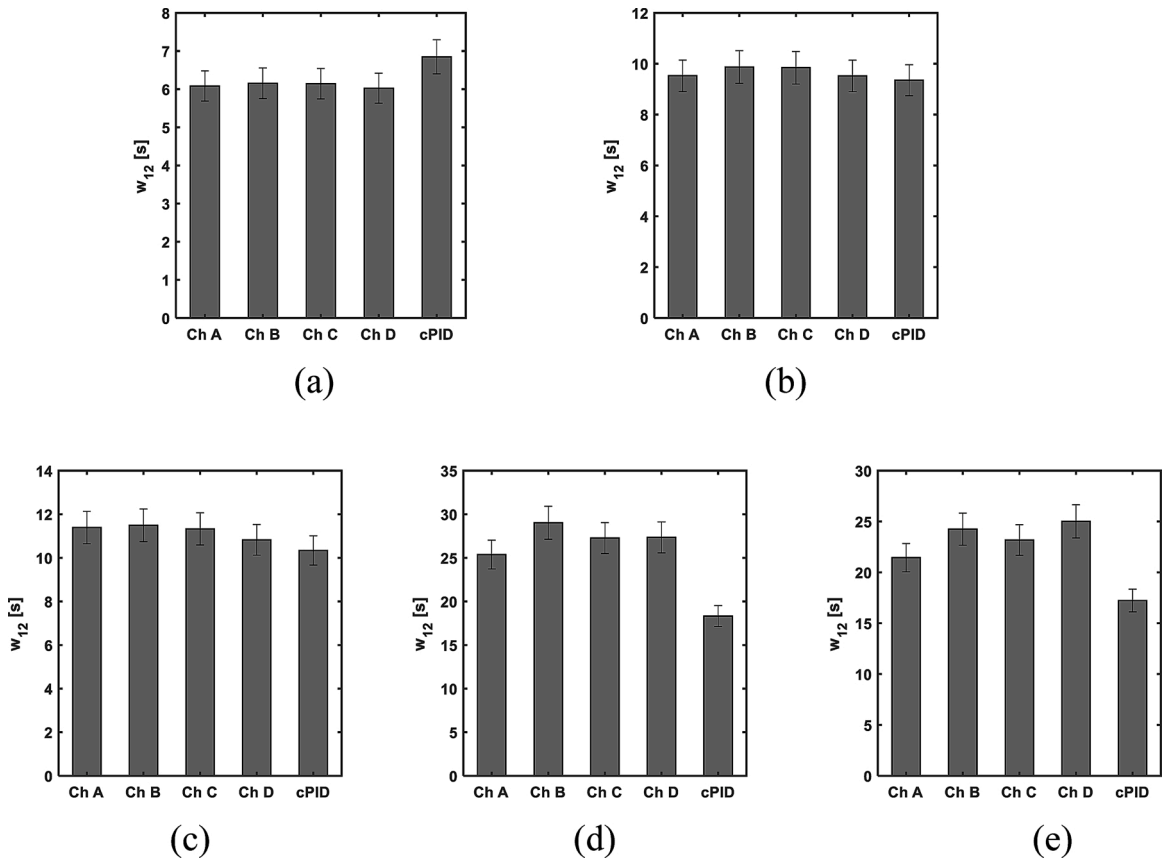

Fig. 9. Chromatographic peak width at half height ($w1/2$) for all channels and commercial PID with a 10 ppm BTEX sample and 30 V on electrodes: a) benzene, b) toluene, c) ethylbenzene, d) m,p-xylenesand e) o-xylene.

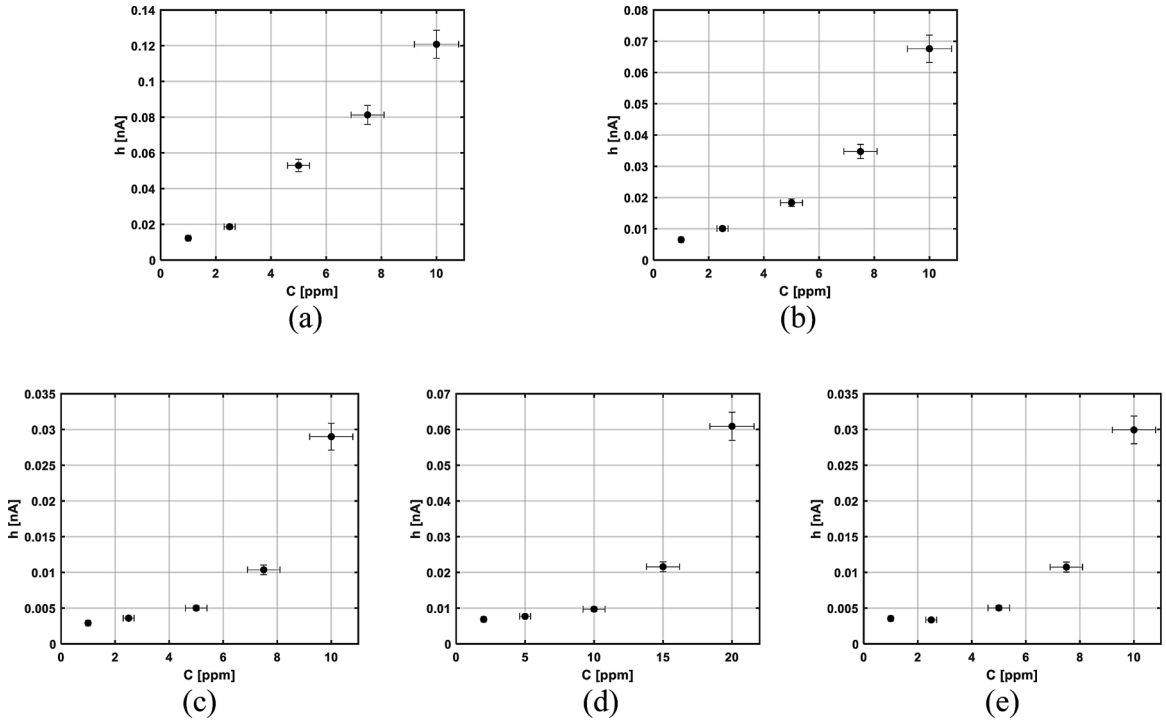

Fig. 10. Calibration curve for GC-μPID (channel D) chromatographic peaks with samples of BTEX at concentration ranging from 1 to 10 ppm and 30 V applied on the electrodes. a) Benzene; b) toluene; c) ethylbenzene; d) m,p-xylenes; e) o-xylene.

Table 2
Detection limit for each species in ppb and pg. Error of 8.9 %.

	Benzene	Toluene	Ethylbenzene	m,p-Xylenes	o-Xylene
D.L. [ppb]	73	138	308	262	254
D.L. [pg]	46	103	266	226	219

4.2. Response curve

The response curve of the GC-μPID (using channel D) for each peak was obtained when applying concentrations ranging from 1 ppm to 10 ppm of BTEX into the gas analyser. The concentration range was obtained using the dilution method described in Section 3.2 and injecting 200 μL of sample from the sampling loop. The peak heights are calculated from the average of two consecutive experiments for each concentration. The height error is 6.5 %, same as mentioned in Section 4.1, and the concentration error has a maximum value of 7.3 %. The response for this range of BTEX concentration is not linear, as shown in Fig. 10.

The concentration detection limit (C_{DL}) can be estimated using Eq. (2) and the signal corresponding to the lowest concentration injected (1 ppm). Considering the noise for the digitally smoothened signal (0.3 pA), the detection limits in concentration and mass units for the four peaks are presented in Table 2. The detection limit in mass units (m_{DL}) is obtained by applying Eq. (3):

$$m_{DL} = \frac{C_{DL} \cdot p_{atm} \cdot V}{R_i \cdot T}, \tag{3}$$

where p_{atm} is the atmospheric pressure (101,325 Pa), V is the sampling loop volume (200 μL), R_i is the specific gas constant for each chemical compound and T is the ambient temperature (300 K).

Notice that the detection limit for toluene is approximately 3.5 times higher than when the detector was tested with direct injection. This can happen because, when the GC system is used, the concentration of the sample spreads while flowing through the separation column and reaches the detector at a lower level.

4.3. Preconcentrator integrated with the GC-μPID sampling loop

As previously demonstrated by Lara-Ibeas et al. (2019), the use of a preconcentration unit (PC) can improve the sensitivity and consequently decrease the detection limit of the gas analyser [26]. An experiment with a PC prototype (developed at ICPEES) was performed as an attempt to improve the detection limit of the GC-μPID. The PC uses an adsorbent to trap the sample and a heating system to release the concentrated sample into the gas analyser. The sampling flow rate for the preconcentration process was 20 mL_n/min applied during 5 min at ambient temperature (~30 °C), the total sample volume being therefore 100 mL. The desorption temperature applied was 270 °C for ~70 s with the sample being injected during 75 s. The PC was integrated into the sampling loop of the gas analyser.

Unfortunately, the preconcentrator prototype suffered a contamination problem due to the presence of unexpected impurities in nitrogen even before the tests with the μPID. This is identified by an unwanted peak measured by the experiment with nitrogen (Fig. 11). After a series of purges with nitrogen, a 5 ppb BTEX sample is injected into the gas analyser with the preconcentrator.

Fig. 11a and b show the chromatograms for the injection of nitrogen and 5 ppb of BTEX, respectively. Since the preconcentrator is applied in this operation, the separation process was adapted and it is 8 min longer compared to the separation process without the preconcentrator. During the purge test with nitrogen (Fig. 11a), it is possible to identify the contamination peak, which hides the benzene signal when the 5 ppb BTEX sample is injected.

Fig. 11b shows the peaks corresponding to the 5 ppb BTEX injection. The pattern of the last three peaks, corresponding to ethylbenzene, m,p-xylene and o-xylene, can be recognized starting at $t = 700$ s. However, the ethylbenzene and o-xylene signal heights are close to the noise level with $SNR < 3$. This means that only toluene and m,p-xylenes peaks are detectable for this experiment, their detection limits being close to 5 ppb (1.87 ng and 2.16 ng with a sample volume of 100 mL, for toluene and m,p-xylenes, respectively). Nonetheless, this shows the potential to a low ppb level detection limit when the μPID is used in a portable GC equipped with a preconcentrator.

5. Conclusions & recommendations

This work presented the characterization of a μPID used with and without a portable GC prototype. The modular feature of the μPID made it possible to test four different channel geometries, with ionization chamber volume ranging from 1.1 to 6.7 μL, and use the same UV lamp. The influence of the geometrical parameters was investigated and showed that the electrode and illumination areas play an important role in the signal magnitude, while the width of the channel has probably a small influence in the signal of the μPID.

When a sample of 100 ppm toluene was injected directly into the μPID at 50 mL_n/min and 30 V applied on the electrodes, it produced a current signal up to ~4 nA (channel D). The signal response time was less than 1 s for all channel designs tested. The higher baseline level for channel A compared to channel B can be due to a larger portion of the electrodes being hit by photons, causing the photoelectric effect. Lamp deterioration can cause significant drop in S_r, near 3 times lower after ~700 h of use. This highlights the importance of the modular feature of the μPID design showed in this work, because the UV lamp can be

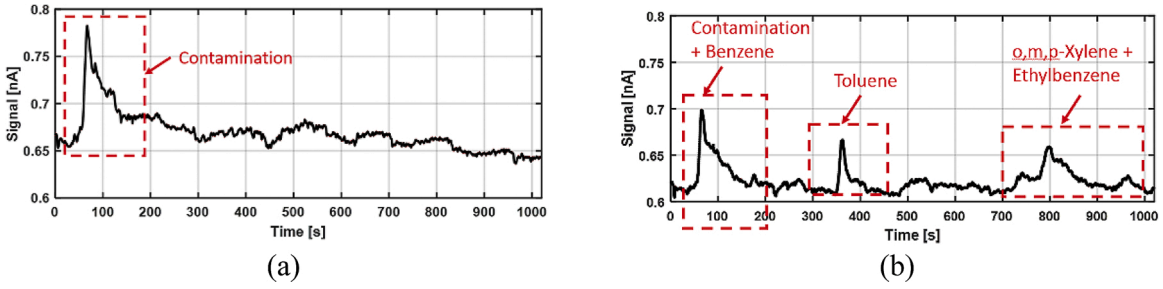

Fig. 11. Chromatogram for GC-μPID equipped with a preconcentrator. Using channel D at 30 V. a) Purge with nitrogen; b) 5 ppb BTEX sample analysis. The sampling flow rate for the preconcentration process was 20 mLn/min at ambient temperature (~30 °C) andthe total sample volume was 100 mL (5 min preconcentration process). The desorption temperature applied was 270 °C for ~70 s with the sample being injected during 75 s.

replaced or removed for maintenance. Considering the linear fit of the response curve from 1–100 ppm of toluene and the lowest noise obtained (0.3 pA), the detection limit for sample direct injection was ~40 ppb.

The response curve of the GC-μPID obtained for channel D from the injection of a 1–10 ppm BTEX sample showed non-linear behaviour, which was more pronounced in the last three peaks of the chromatogram. The detection limit obtained for benzene, toluene, ethylbenzene, m,p-xylenes and o-xylene peaks are 73, 138, 308, 262 and 254 ppb, respectively. For the four microchannels tested, no significant variation of peak width was observed and can be explained for the relatively high sample volume eluting from the separation column. Despite the contamination issues in the preconcentrator prototype, it was still possible to reach low ppb detection limit for toluene when the PC was integrated into the GC sampling system.

Future work could be done to develop a portable amplifier for the μPID so it can be easily integrated into the GC prototype for field analysis. Practical study of the influence of humidity in the sensor response is necessary to apply filters. Another important future step is to integrate the μPID into a lab-on-a-chip gas chromatograph with preconcentrator, this will enable to increase the portability of the whole gas analyser system. A modular μGC-μPID system should be built in the future and can improve maintenance of overall gas analyser and increase the flexibility of the application, since specific parts can be added according to application needs.

CRediT authorship contribution statement

Gustavo Coelho Rezende: Conceptualization, Methodology, Software, Validation, Formal analysis, Investigation, Resources, Data curation, Writing - original draft, Writing - review & editing, Visualization, Project administration. **Stéphane Le Calvé:** Conceptualization, Methodology, Validation, Resources, Writing - review & editing, Supervision, Project administration, Funding acquisition. **Jürgen J. Brandner:** Conceptualization, Methodology, Validation, Resources, Writing - review & editing, Supervision, Project administration, Funding acquisition. **David Newport:** Conceptualization, Methodology, Validation, Resources, Writing - review & editing, Supervision, Project administration, Funding acquisition.

Declaration of Competing Interest

The authors report no declarations of interest.

Acknowledgements

This study was developed during the ITN Research Project, MIGRATE, supported by European Community H2020 Framework under the Grant Agreement No. 643095.

Appendix A. Supplementary data

Supplementary material related to this article can be found, in the online version, at doi:https://doi.org/10.1016/j.snb.2020.128667.

References

[1] N.E. Klepeis, W.C. Nelson, W.R. Ott, J.P. Robinson, A.M. Tsang, P. Switzer, J. V. Behar, S.C. Hern, W.H. Engelmann, The National Human Activity Pattern Survey (NHAPS): a resource for assessing exposure to environmental pollutants, J. Exposure Anal. Environ. Epidemiol. 11 (2001) 231–252.

[2] European Comission, Indoor Air Pollution: New EU Research Reveals Higher Risks Than Previously Thought, Eur. Com., 2003. IP/03/1278. http://europa.eu/rapid/press-release_IP-03-1278_en.htm#file.tmp_Foot_1 (Accessed March 26, 2019).

[3] L.A. Wallace, E. Pellizzari, B. Leaderer, H. Zelon, L. Sheldon, Emissions of Volatile Organic Compounds from Building Materials and Consumer Products, 1987, https://doi.org/10.1016/0004-6981(87)90017-5.

[4] WHO, Air Quality Guidelines for Europe, 2nd ed., 2000, https://doi.org/10.1007/BF02986808.

[5] WHO, WHO Guidelines for Indoor Air Quality: Selected Pollutants, 2010, https://doi.org/10.1186/2041-1480-2-S2-I1.

[6] European Comission, DIRECTIVE 2000/69/EC OF THE EUROPEAN PARLIAMENT AND OF THE COUNCIL of 16 November 2000 relating to limit values for benzene and carbon monoxide in ambient air., Off. J. Eur. Communities. (2000). doi: 10.1016/j.jclepro.2010.02.014.

[7] Ministère de L'Ecologie, Ministère de l'Ecologie. Décret no 2011-1727 du 2 décembre 2011 relatif aux valeurs-guides pour l'air intérieur pour le formaldéhyde et le benzène, J. Off. La République Française. (2011). doi:10.1051/dmbd/120108.

[8] C. Poole, Gas Chromatography, first ed., Elsevier, 2012.

[9] BTEX analyzer with PID detector: chromaPID, Chromatotec, (n.d.). http://www.chromatotec.com/BTEX,analyzer,with,PID,detector,chromaPID-Article-138-ChromaGC-Product-14.html (Accessed July 19, 2018).

[10] MODEL GC955-600, ET enviro Technology Services, (n.d.). http://www.et.co.uk/products/air-quality-monitoring/continuous-gas-analysers/synspec-gc955-601-btx/ (Accessed July 19, 2018).

[11] Baseline MOCON 8900, (2019). http://products.baseline-mocon.com/Asset/D010.3_Series 8900_GC_0217.pdf.

[12] S. Khan, D. Newport, Development of a Toluene Detector Based on Deep UV Absorption Spectrophotometry Using Glass and Aluminum Capillary Tube Gas Cells with a LED Source, 2019, https://doi.org/10.3390/mi10030193.

[13] G.C. Rezende, S. Le Calvé, J.J. Brandner, D. Newport, Micro photoionization detectors, Sens. Actuators B Chem. 287 (2019) 86–94, https://doi.org/10.1016/j.snb.2019.01.072.

[14] OI Analytical, Model 4430, Photoionization Detector Operator's Manual, 2009 (Accessed July 20, 2018), http://aimanalytical.com/Manuals/PIDFIDmanual.pdf.

[15] SRI Instruments, 8690-0040 PID Detector, 2018 (Accessed October 4, 2018), https://www.srigc.com/home/product_detail/pid—photo-ionization-detector.

[16] C. Liaud, N.T. Nguyen, R. Nasreddine, S. Le Calvé, Experimental performances study of a transportable GC-PID and two thermo-desorption based methods coupled to FID and MS detection to assess BTEX exposure at sub-ppb level in air, Talanta 127 (2014) 33–42, https://doi.org/10.1016/j.talanta.2014.04.001.

[17] Baseline MOCON, (2019). http://www.baseline-mocon.com (Accessed July 6, 2018).

[18] J. Sun, F. Guan, D. Cui, X. Chen, L. Zhang, J. Chen, An improved photoionization detector with a micro gas chromatography column for portable rapid gas chromatography system, Sens. Actuators B Chem. 188 (2013) 513–518, https://doi.org/10.1016/j.snb.2013.07.066.

[19] H. Zhu, R. Nidetz, M. Zhou, J. Lee, S. Buggaveeti, K. Kurabayashi, X. Fan, Flow-through microfluidic photoionization detectors for rapid and highly sensitive vapor detection, Lab Chip 15 (2015) 3021–3029, https://doi.org/10.1039/C5LC00328H.

[20] J. Lee, M. Zhou, H. Zhu, R. Nidetz, K. Kurabayashi, X. Fan, Fully automated portable comprehensive 2-dimensional gas chromatography device, Anal. Chem. 88 (2016) 10266–10274, https://doi.org/10.1021/acs.analchem.6b03000.

[21] M. Akbar, M. Restaino, M. Agah, Chip-scale gas chromatography: from injection through detection, Microsyst. Nanoeng. 1 (2015) 15039, https://doi.org/10.1038/micronano.2015.39.

[22] H. Zhu, M. Zhou, J. Lee, R. Nidetz, K. Kurabayashi, X. Fan, Low-power miniaturized helium dielectric barrier discharge photoionization detectors for highly sensitive vapor detection, Anal. Chem. 88 (2016) 8780–8786, https://doi.org/10.1021/acs.analchem.6b02180.

[23] S. Narayanan, G. Rice, M. Agah, A micro-discharge photoionization detector for micro-gas chromatography, Microchim. Acta 181 (2014) 493–499, https://doi.org/10.1007/s00604-013-1146-9.

[24] G.C. Rezende, S. Le Calvé, J. Brandner, D. Newport, Micro milled microfluidic photoionization detector for volatile organic compounds, Micromachines 10 (2019), https://doi.org/10.3390/mi10040228.

[25] R. Nasreddine, V. Person, C.A. Serra, S. Le Calvé, Development of a novel portable miniaturized GC for near real-time low level detection of BTEX, Sens. Actuators B Chem. 224 (2016) 159–169, https://doi.org/10.1016/j.snb.2015.09.077.

[26] I. Lara-Lbeas, A. Rodríguez-Cuevas, C. Andrikopoulou, V. Person, L. Baldas, S. Colin, S. Le Calvé, Sub-ppb level detection of BTEX gaseous mixtures with a compact prototype GC equipped with a preconcentration unit, Micromachines 10 (2019), https://doi.org/10.3390/mi10030187.

Dr. Gustavo Coelho Rezende is a Marie Skłodowska Curie alumni who worked on the MIGRATE project and received his PhD degree in 2020 from the University of Limerick (Limerick, Ireland). In his PhD, he developed a photoionization detector prototype to be used for air quality monitoring. During the MIGRATE project, in 2018, he joined Karlsruhe Institute of Technology for 4 months as a guest researcher to focus on the fabrication of the photoionization detector. He also worked in collaboration with a French Startup (In'Air Solutions) to integrate the sensor prototype into a portable gas chromatograph.

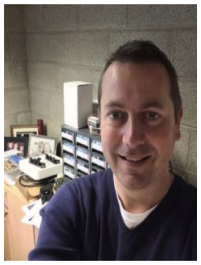

Stéphane Le Calvé is currently research Director at the French National Centre for Scientific Research (CNRS), the Head of the Department of molecular and analytical chemistry and the Head of the group of atmospheric physical chemistry at the Institute of Chemistry and Processes for Energy, Environment and Health (ICPEES) in Strasbourg. He received his PhD degree specialized in atmospheric sciences at University of Orléans (France) in 1998 and spent his post-doc at University College of Dublin (Ireland). Since 1999, he is a permanent researcher at CNRS in Strasbourg. For almost ten years, he was member of the scientific program PRIMEQUAL led by ADEME and the French Ministry of the Environment. Initially, his work focused on atmospheric chemistry, kinetics and reactivity in the gas and heterogeneous phases, ice chemistry, gas-liquid equilibrium and adsorption of Volatile Organic Compounds. At present, his scientific researches are dedicated to the development of new microfluidic analytical tools including design, manufacturing, experimental validation under controlled laboratory conditions and field measurement campaigns, in order to enhance the air quality monitoring.

Prof. Dr.-Ing. habil. Juergen J. Brandner studied Chemistry at University of Heidelberg and Electrical Engineering at Technical University of Karlsruhe. He obtained a PhD in Mechanical Engineering at the Technical University of Karlsruhe and a habilitation in Micro Process Engineering at Technical University of Dresden. Currently he is head of the Microstructures and Process Sensors Group at KIT and professor for Micro Process Engineering at Technical University of Dresden. He is also leading the Karlsruhe Nano Micro Facility (KNMF) at KIT (http://www.knmf.kit.edu). Prof. Brandner received the Linde-Award 2009 of Technical University of Dresden (Best Habilitation Thesis) as well as the NEULAND Innovation Award of KIT in 2014, 2015 and 2016. He is working in microstructure devices for about 20 years now. He provides lectures in Micro Process Engineering at Technical University of Dresden, Miniaturized Heat Exchanger Devices at Karlsruhe Institute of Technology. He is author or co-author of about 360 publications in international journals and international conferences as well as contributing to 12 textbooks.

Dr. David Newport is currently a Senior Lecturer at the University of Limerick, with a background in thermofluids centred on thermal management of electronic systems and natural convection heat transfer. At present David's research is focussed on Process and Biomedical applications for microfluidics, with an emphasis on experimental methods. He has a long standing interest in the development of optical metrology techniques for microfluidic flows, in particular interferometry. His current research interests include advection of cell suspensions in microflows, in-vitro models of the blood-brain-barrier, detection of VOCs in air using miniaturized sensors and micro-vascular flows.